Int. J. Electrochem. Sci., 7 **(2012)** 9984 - 9996

International Journal of
ELECTROCHEMICAL
SCIENCE
www.electrochemsci.org

Synthesis and Capacitive Performances of Graphene/N-Doping Porous Carbon Composite with High Nitrogen Content and Two-Dimensional Nanoarchitecture

Min Zhou, Xingwei Li, Jiajia Cui, Tingting Liu, Tingwei Cai, Huichen Zhang, Shiyou Guan[*]

Shanghai Key Laboratory of Advanced Polymeric Materials, Key Laboratory for Ultrafine Materials of Ministry of Education, School of Materials Science and Engineering, East China University of Science and Technology, Mei Long Road 130, Shanghai 200237, P.R.China
[*]E-mail: syguan@ecust.edu.cn

Received: 21 August 2012 / *Accepted:* 11 September 2012 / *Published:* 1 October 2012

Graphene/N-doping porous carbon composite (G-CN_x, 0<x<1) with high nitrogen content (13.51 wt%) and unique two-dimensional nanoarchitecture was prepared using ionic liquids (1-ethyl-3-methylimidazolum dicyanamide) as nitrogen-rich carbon precursors and graphene/porous silica composite as a template with a simply nanocasting technology. Electrochemical evaluation showed that G-CN_x with nitrogen content of 13.51 wt% manifested a significantly enhanced capacitive performances compared to G-CN_x with low nitrogen content (7.15 wt%) and graphene/porous carbon composite (G-C) in 1M H_2SO_4 electrolyte. The specific capacitance of G-CN_x with nitrogen content of 13.51 wt% reached 206 F g^{-1} at a current density of 0.1 A g^{-1}, much larger than those of G-CN_x with nitrogen content of 7.15 wt% (161 F g^{-1}) and G-C (69 F g^{-1}). The improved capacitive performances may due to the Faradaic redox reaction and the enhanced surface wettability by electrolyte, which related to the nitrogen functionalities. G-CN_x with high nitrogen content is great promise in the areas of electronics and sensors as well as energy storage and conversion.

Keywords: Graphene, N-doping porous carbon, 1-ethyl-3-methylimidazolum dicyanamide, capacitive performances

1. INTRODUCTION

Graphene-based composites are of great interests due to their extraordinary properties, such as large thermal conductivity, superior mechanical properties, and unusual electrical properties generated from their long-range π-conjugation [1-5]. Graphene/porous carbon composite (G-C) is a novel two-dimensional nanomaterial in which monolayer graphene or few-layer graphene is fully separated by a porous carbon shell with nanoscale dimension in thickness [6]. The resulting G-C, which posses a

large aspect ratio, high surface area, and excellent electrical conductivity, has attracted tremendous attention owing to their potential applications in the areas of electronics and sensors as well as energy storage and conversion.

G-C was first fabricated by Yang *et al.* using graphene/porous silica composite (G-silica) as a template and sucrose as a carbon precursor with a nanocasting technology in 2010 [6]. Recently, they successfully developed an efficient strategy for the fabrication of graphene/N-doping porous carbon composite (G-CN_x, $0<x<1$) by employing ethylenediamine and carbon tetrachloride as CN precursors instead of sucrose, and in which the porous carbon shell contained moderate content of nitrogen [7]. The incorporation of nitrogen in the carbon nanostructure enhances many properties of carbon, including the basicity, oxidation stability, catalytic activity, conductivity as well as energy storage and conversion, because the electron-rich nitrogen atoms can modify the band structure of the material [8-10]. The valence band is lowered, thus the material is chemically more stable, and the electron density at the Fermi level is increasing. G-CN_x has been demonstrated to have high electrocatalytic activity and selectivity when using as metal-free catalysts for the oxygen reduction reactions [7]. However, the synthesis of G-CN_x with high nitrogen content is very difficult using ethylenediamine and carbon tetrachloride as CN precursors because of the low molar ratios N/C and the large extent of the thermal decomposition of functional groups containing nitrogen during the thermal treatment. In order to obtain N-doping porous carbon shell with a certain degree of graphitization, pyrolysis must be carried out at $\geq$800 ^{o}C, and the overall nitrogen content of as-prepared G-CN_x is below 10 wt%.

In last two decades, various applications of ionic liquids, including catalysis [11], chemical synthesis [12], electrochemistry [13], separation [14] and advanced materials [15], have been developed for their intrinsic properties such as negligible vapor pressure, high thermal, chemical, and electrochemical stabilities and wide liquid temperature ranges. Recently, some groups have successfully demonstrated the preparation of nitrogen-rich carbons using task specific ionic liquids (TSILs) as precursors [16-20]. TSILs, such as 1-ethyl-3-methylimidazolium dicyanamide (EMIM-dca, 39.5 wt% N), are shown to be versatile precursors for the generation of nitrogen-doped carbons with a high nitrogen content, an equal distribution of nitrogen and carbon and a graphite-like structure when heating at 600 ^{o}C [16]. Meanwhile, TSILs exhibit practically no vapor pressure, and can be carbonized under constant nitrogen flow in ambient pressure without evaporation. In contrast, most CN precursors including ethylenediamine and carbon tetrachloride should be polymerized before carbonization [21].

Herein, synthesis of G-CN_x with nitrogen content of 13.51 wt%, unique two-dimensional nanoarchitecture and a certain degree of graphitization was reported, which was obtained by using suitable ionic liquid (EMIM-dca) as nitrogen-rich carbon precursors, and the carbonization was only carried out at 600 ^{o}C.

As the electrode material, two-dimensional nanoarchitectures (nanosheets) are of great interest in clean energy storage and conversion, in particular supercapacitor, due to its shortened paths for fast electrolyte ion diffusion and large exposed surface offering more active sites for charge storage [22]. Also the presence of some chemical functionality containing heteroatoms, such as nitrogen, gives carbon materials basic character and thus enhances the capacitance with pseudocapacitance (which generally originates from the faradaic interactions between the ions of electrolytes and the chemical

functionality) [23-29] and enhanced surface wettability by electrolyte (which ensures a complete utilization of the exposed surfaces for charge storage) [23].

The capacitive performances of as-prepared G-CN_x were studied by cyclic voltammetry and galvanostatic charge/discharge. Results showed that the specific capacitance of G-CN_x with high nitrogen content (13.51 wt%) reached 206 F g^{-1} at a current density of 0.1 A g^{-1} in 1M H_2SO_4 electrolyte, and those of G-CN_x with low nitrogen content (7.15 wt%) and G-C were 161 F g^{-1} and 69 F g^{-1}, respectively.

2. EXPERIMENTAL PART

2.1 Synthesis

The scheme for the preparation of G-CN_x or G-C is presented in Fig. 1. G-silica was first fabricated by the hydrolysis of tetraethylorthosilicate (TEOS) on the surface of graphene oxide (GO) with the help of a cationic surfactant (cetyltrimethyl ammonium bromide, CTAB) and reduction of GO to graphene by annealing under nitrogen. Precursor was subsequently impregnated into the pores of G-silica and pyrolysised. G-CN_x or G-C was obtained after etching of silica, and in which G-CN_x using EMIM-dca and a mixture of ethylenediamine and carbon tetrachloride as CN precursors defined as G-CN_x-1 and G-CN_x-2, respectively.

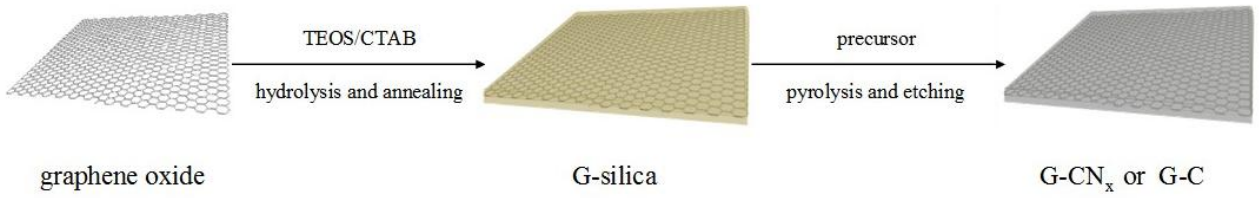

Figure 1. The scheme for the preparation of G-CN_x or G-C.

Preparation of G-silica was as follows: 120 mg of GO, which was synthesized from natural graphite flakes by a modified Hummers method [30], was firstly suspended in an aqueous solution containing CTAB (4 g) and NaOH (160 mg), and then ultrasonically treated for 3 h. After stirring for 2 h at 40 ^oC, TEOS (4 ml) was slowly added to the above mixture, and the suspension was again stirred for 12 h. Graphene oxide/porous silica composite (GO-silica) was obtained by separating, washing and drying. G-silica was produced by the pyrolysis of GO-silica at 800 ^oC for 3 h under nitrogen.

Preparation of G-CN_x-1 was as follows: EMIM-dca was infiltrated into the G-silica by vigorously stirring appropriate amount of G-silica (0.5 g) in EMIM-dca under vacuum at 150 ^oC for 10 h. The EMIM-dca is structured as follows:

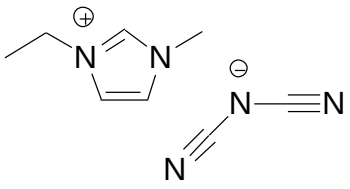

$C_8H_{11}C_5$

Any excess of EMIM-dca was eliminated by vacuum filtration. For carbonization of EMIM-dca, G-silica contained EMIM-dca was first heated to 500 ^oC and kept at this temperature for 1 h, and then the temperature was increased to 600 ^oC and kept at this temperature for 3 h under flowing nitrogen atmosphere. The same impregnation and carbonization procedure was repeated once more to ensure full use of the pores. The obtained black powder was stirred in 2M NaOH aqueous solution to dissolve the silica template. After filtration and washing with de-ionized water several times, the product was dried in a vacuum drying oven at 80 ^oC for 24 h.

Preparation of G-CN_x-2 was as follows: 0.5 g of G-silica was added to a mixture of ethylenediamine ($NH_2CH_2CH_2NH_2$, 2.2 g) and carbon tetrachloride (CCl_4, 5.4 g). The resultant mixture was refluxed and stirred at 90 ^oC for 6 h. Then, the sample obtained was placed in a vacuum drying oven at 100 ^oC for 10 h and heat-treated under flowing nitrogen atmosphere at 800 ^oC for 5 h. G-CN_x-2 was obtained after the dissolution of the silica framework in 2M NaOH aqueous solution. After filtration and washing with de-ionized water several times, the product was dried in a vacuum drying oven at 80 ^oC for 24 h.

Preparation of G-C was as follows: 0.5 g of G-silica was added to a solution dissolved 0.625 g of sucrose ($C_{12}H_{22}O_{11}$) and 0.038 ml of H_2SO_4 (98 wt%) in 2.5 ml of H_2O. The mixture was placed in a vacuum drying oven for 6 h at 100 ^oC, and subsequently the oven temperature was increased to 160 ^oC and maintained for 6 h. The sample obtained was treated again at 100 ^oC and 160 ^oC after the addition of 0.4 g of sucrose, 0.024 ml of H_2SO_4 (98 wt%) in 2.5 ml of H_2O. The carbonization was completed by pyrolysis at 900 ^oC for 3 h under flowing nitrogen atmosphere. The product after pyrolysis was washed with 2M NaOH aqueous solution to remove the silica template. After filtration and washing with de-ionized water several times, the product was dried in a vacuum drying oven at 80 ^oC for 24 h.

2.2 Characterization

The observations of morphology were performed using a JSM-6360LV scanning electron microscope (SEM, JEOL, Japan) and a JEM-1400 transmission electron microscope (TEM, JEOL, Japan). The Brunauer-Emmett-Teller (BET) method was used to determine the surface area by measuring the adsorption of N_2 at 77 K using a NOVA 4200e (Quantachrome, USA) instrument. Before measurement, the sample was degassed at a temperature of 180 ^oC for 8 h. Powder X-ray diffraction (XRD) pattern was obtained on a D / MAX 2550VB / PC diffractometer (Rigaku, Japan) using Cu Kα radiation (λ=0.154 nm). Raman spectrum was recorded using an InVia Raman microscope (Renishaw, UK) with 514.5 nm diode laser excitation. The elemental analysis was carried out on CHNS Vario ELIII (Elementar Analysen systeme GmbH, Germany) by a conventional CHN

combustion method based on the burn off of the sample and TCD analysis of nitrogen and carbon mass percentage from the evolved gases.

The capacitive performances were performed by a CHI660D potentiostat/galvanostat at room temperature (20 ^{o}C). A conventional three-electrode cell was used, in which platinum wire and Ag/AgCl (saturated KCl solution) electrodes were used as counter and reference electrodes, respectively. The working electrode was prepared by mixing G-CN_x-1 or G-CN_x-2 or G-C with acetylene black and polytetrafluoroethylene in a mass ratio of 8:1:1 and pressing onto titanium mesh at a pressure of 5 Mpa. The used electrolyte was 1M H_2SO_4 aqueous solution, and the working electrode was soaked in the electrolyte for 24 h before measurement.

3. RESULTS AND DISCUSSIONS

3.1 Morphology

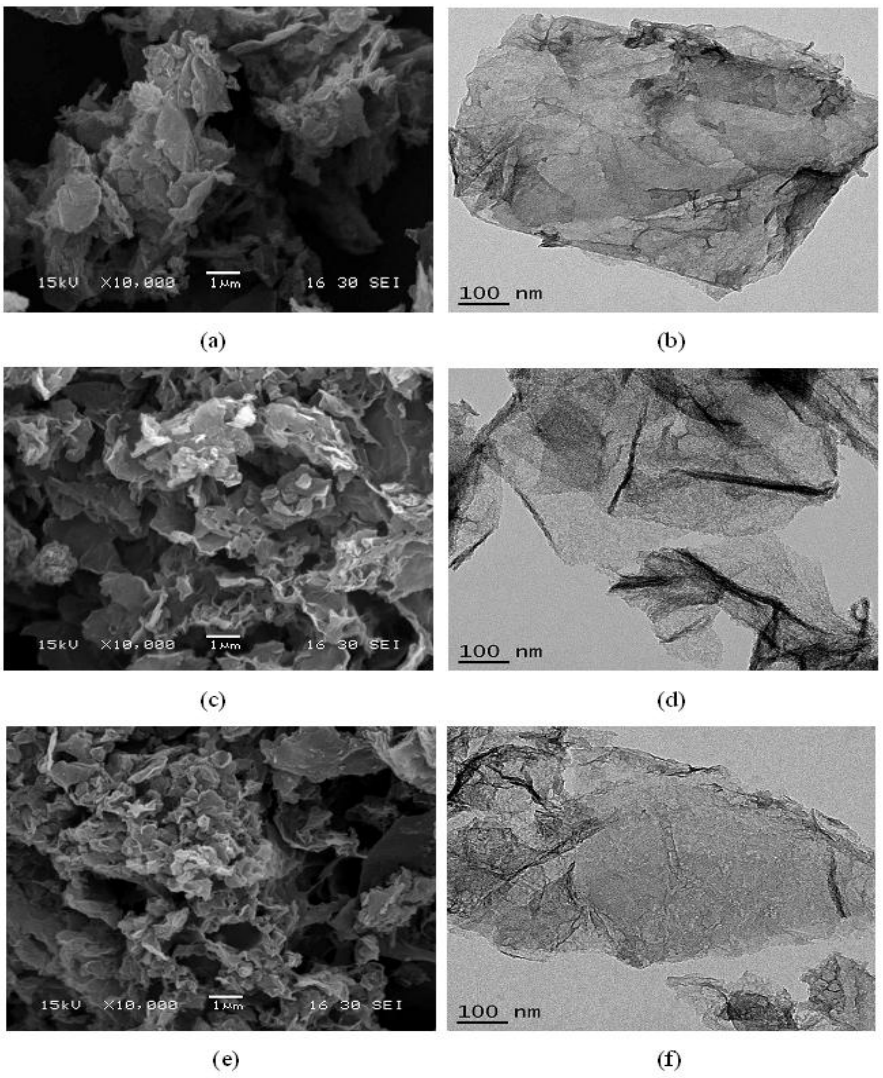

Figure 2. SEM and TEM of G-CN_x-1 (a, b), G-CN_x-2 (c, d) and G-C (e, f).

SEM and TEM of G-CN_x-1, G-CN_x-2 and G-C were given in Fig. 2. Large amounts of nanosheets with morphology similar to that of graphene were observed in the above samples, and the nanosheets appeared a loosely packed structure. Although most of the nanosheets became crumpled due to the shrinkage of samples during the thermal treatment process, TEM images revealed they still maintained the large aspect ratio. It was worth to noting that no apparent carbon deposition was found in either SEM or TEM visualizations, indicating that the precursors were mostly infiltrated into the G-silica template channels.

3.2 Pore structure, specific surface area, and nitrogen content

In order to investigate the pore structure and specific surface area, the nitrogen adsorption-desorption isotherms of G-CN_x-1, G-CN_x-2 and G-C were carried out, as shown in Fig. 3. From Fig. 3, it was found that all samples displayed a type IV isotherm with a hysteresis loop at medium and high relative pressures (P/P_0=0.40 to 0.99) caused by capillary condensation, indicating the existence of large numbers of mesopores and macropores. In addition, an increase of N_2 adsorption was observed at low relative pressure, suggesting the presence of micropores. Therefore, it can be concluded that G-CN_x-1, G-CN_x-2 and G-C possess a hierarchical porous structure including micropores, mesopores and macropores. This is a result of the replication of the porous template (G-silica) and continuous decomposition of the precursor during thermal treatment. It was also noted that the adsorption isotherms of G-CN_x-1, G-CN_x-2 and G-C were clearly different at a high relative pressure, which should be attributed to the incorporation of nitrogen into the carbon framework and a larger pore size of G-CN_x-1 and G-CN_x-2. The introduction of nitrogen can improve the surface wettability of the carbon material [23], thereby affecting the interaction between adsorbent and adsorbate.

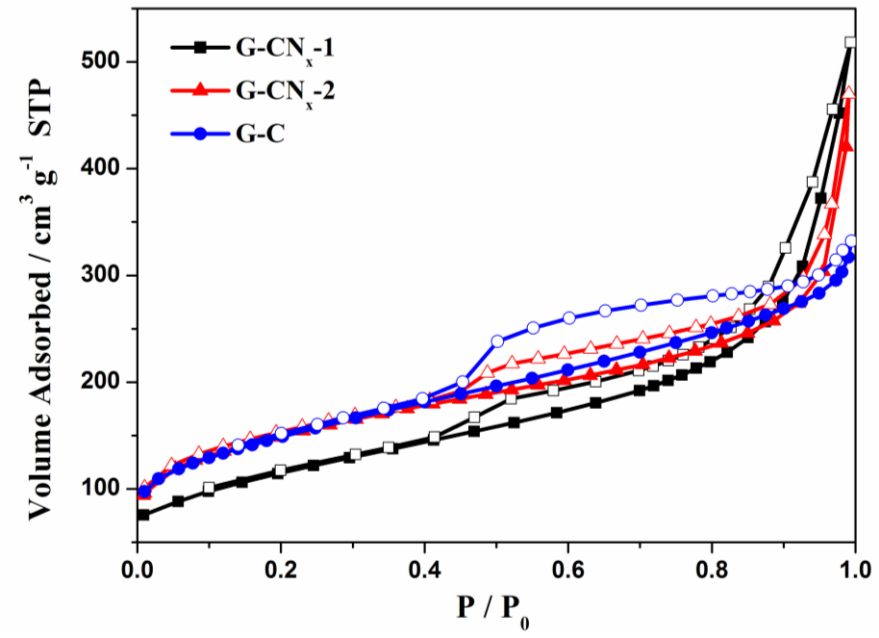

Figure 3. Nitrogen adsorption-desorption isotherms of G-CN_x-1, G-CN_x-2 and G-C.

BET specific surface area and pore volume of all samples were listed in Table 1. Table 1 showed that BET specific surface area of G-CN_x-1 (404 m^2 g^{-1}) was lower than that of G-C (529 m^2 g^{-1}) or G-CN_x-2 (502 m^2 g^{-1}), while the pore volume was the largest up to 0.76 cm^3 g^{-1}. Although specific surface area of G-C and G-CN_x-2 was near, the pore volume of G-C was 0.46 cm^3 g^{-1}, and that of G-CN_x-2 was 0.73 cm^3 g^{-1}.

It was worth to noting that different precursors used in our work had different surface energy, thus the wettibility, and their filling was different, which may be regarded to be responsible for the different pore structure and specific surface, although G-silica templates were the same.

The contents of nitrogen of all samples were also listed in Table 1. 13.51wt% of the nitrogen content was presented in G-CN_x-1, which was obviously higher than that of G-CN_x-2. The high content of nitrogen in the carbon framework is ascribed to the EMIM-dca precursor which possesses high nitrogen content (39.5wt% N) [16].

Table 1. Chemical composition and porous properties of G-CN_x-1, G-CN_x-2 and G-C.

Sample	N wt%	S_{BET} (m^2 g^{-1})	Pore volume (cm^3 g^{-1})
G-CN_x-1	13.51	404	0.76
G-CN_x-2	7.15	502	0.73
G-C	—	529	0.46

3.3 XRD pattern and Raman spectra

To examine the graphitic character of G-CN_x-1, G-CN_x-2 and G-C, XRD pattern was performed. As illustrated in Fig. 4, all the samples exhibited a broad reflection at a 2θ value of about 24 ° and a weak reflection centered around 43 °, which correspond to the (002) and (10) facets of graphitic-type carbon structure, respectively [31]. The (10) peak intensity of G-C was stronger than those of G-CN_x-1 and G-CN_x-2, revealing a higher graphitization degree using sucrose as precursor carbonizing at a relatively high temperature of 900 ^oC, which was also confirmed from the following Raman spectra, shown in Fig. 5.

From Fig. 5, it was seen that all samples showed two main peaks centered at around 1350 and 1580 cm^{-1}, which were designated as the D band and the G band [32], respectively. The G band is associated with the allowed E_{2g} optical modes of the Brillouin zone center of the crystalline graphite [33], while the D band usually appears when the graphite structure is seriously destroyed [34,35]. The relative intensity ratio of the D and G bands, I_D/I_G, can give information about the perfection of the graphite layer structure [36]. As the I_D/I_G ratio increases, the defect structure increases and the degree of graphitization becomes less [37]. As shown in Table 2, the I_D/I_G ratio of G-C was the lowest, and G-CN_x-1 had a slightly higher degree of graphitization than G-CN_x-2 although the carbonization temperature of G-CN_x-1 (600 ^oC) was lower than that of G-CN_x-2 (800 ^oC).

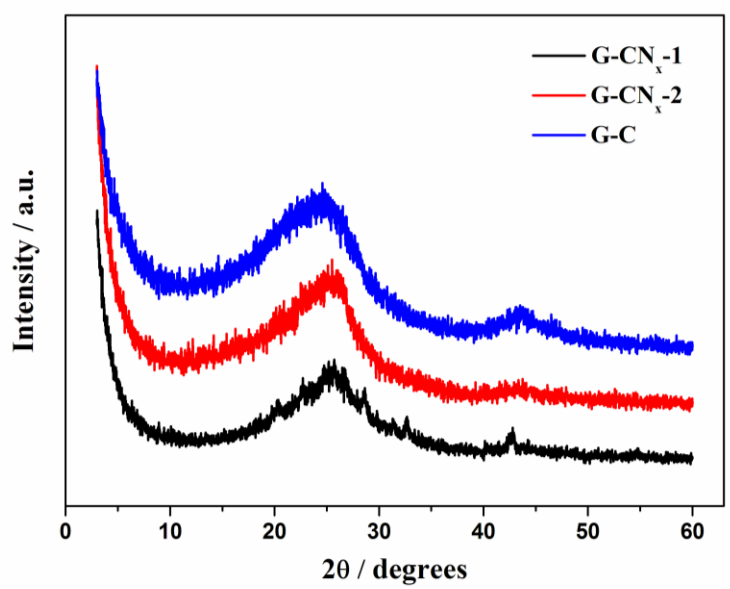

Figure 4. XRD pattern of G-CN$_x$-1, G-CN$_x$-2 and G-C.

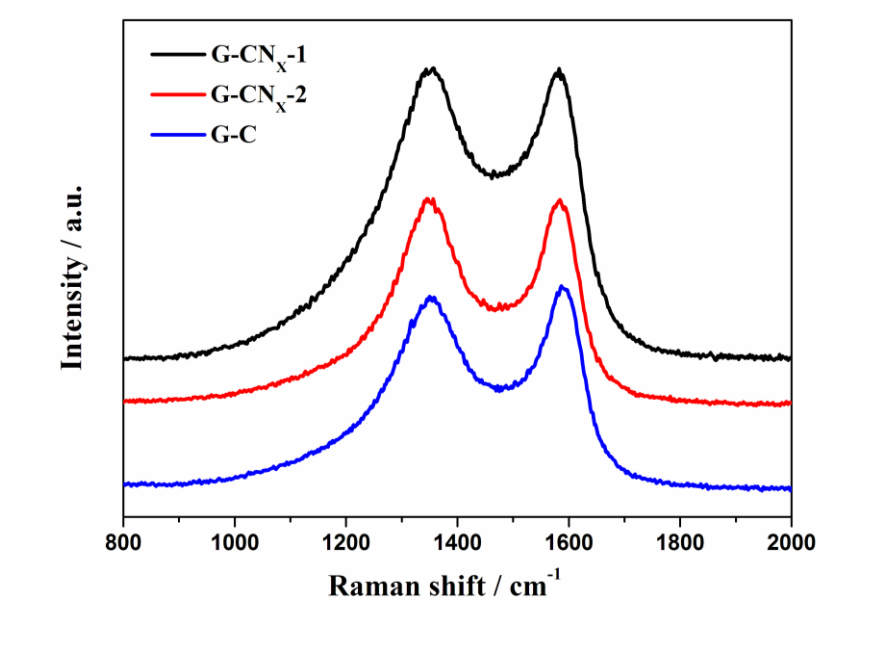

Figure 5. Raman spectra of G-CN$_x$-1, G-CN$_x$-2 and G-C.

Table 2. I_D/I_G of G-CN$_x$-1, G-CN$_x$-2 and G-C obtained from Raman spectra.

Sample	I_D/I_G
G-CN$_x$-1	1.66
G-CN$_x$-2	1.75
G-C	1.59

3.4 Electrochemical capacitance performances

Cyclic voltammetry and galvanostatic charge/discharge were used to characterize the capacitive properties of our carbon materials. The voltammetry characteristics and galvanostatic charge/discharge curves (Fig. 6, 7 and 8) for these samples in acidic media (1M H_2SO_4) showed good capacitor response even at a high loading.

Fig. 6 displayed cyclic voltammetry curves of G-CN_x-1, G-CN_x-2 and G-C recorded at various scan rates (1-20 mV s^{-1}). Unlike the cyclic voltammetry curves of G-C with a rectangular-like shape (Fig. 6c), the cyclic voltammetry curves of G-CN_x-1 (Fig. 6a) and G-CN_x-2 (Fig. 6b) indicated that the capacitive response came from not only electric double-layer contribution, which directly related with the porous structure, but also redox reactions, which related to the heteroatom functionalities of the materials. The nearly rectangular shapes were kept at 10 mV s^{-1}, whereas the characteristics were slightly aggravated at 20 mV s^{-1} (Fig. 6a, b). Such limitations at higher loading were also the proof that faradaic reactions were involved. Nitrogen functionalities have generally basic characterization, inducing electron–donor properties [29]. These electrochemically active centers contribute to the pseudocapacitance, which generally originates from the Faradaic interactions between nitrogen-containing functional groups and the protons from the H_2SO_4 aqueous solution during the charge/discharge process [23,24].

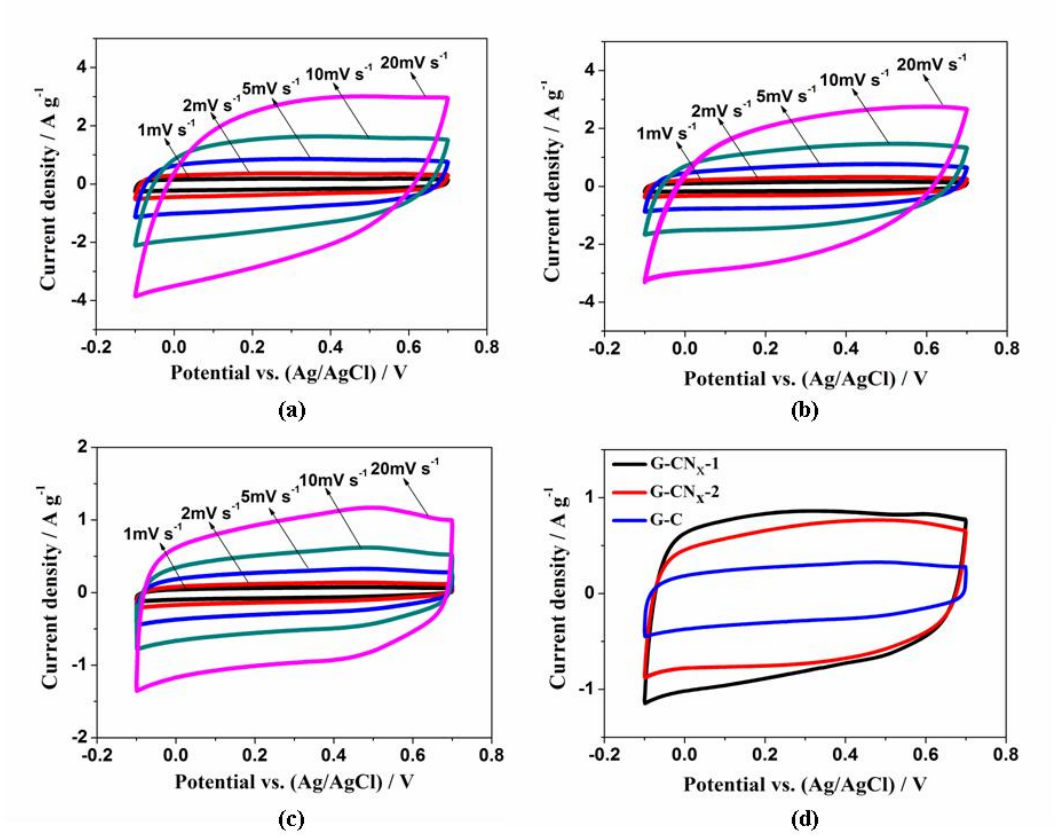

Figure 6. Cyclic voltammetry curves of G-CN_x-1 (a), G-CN_x-2 (b), and G-C (c) with various scan rates (1-20 mV s^{-1}) and G-CN_x-1, G-CN_x-2, G-C at a scan rate of 5 mV s^{-1} (d) in an electrolyte of 1M H_2SO_4 aqueous solution.

Fig. 6d showed cyclic voltammetry curves of G-CN_x-1, G-CN_x-2 and G-C at the same scan rate (5 mV s^{-1}). The current density increased obviously with increasing nitrogen content, indicating G-CN_x-1 with high nitrogen content had higher capacity than G-CN_x-2 and G-C.

The improved capacitive performance also could be observed in the galvanostatic charge/discharge curves (Fig. 7). All the samples clearly exhibited ideal triangle charge/discharge curves, indicating the low equivalent series resistance of the electrodes under this loading current density (0.1 A g^{-1}). Their specific capacitance obtained from the galvanostatic charge/discharge curve can be calculated according to the following equation:

$$Cm = \frac{I \cdot t}{m \cdot \Delta V}$$

Where C_m is specific capacitance [F g^{-1}], I is galvanostatic charge/discharge current [A], t is the discharge time, m is the mass of active material [g] , and ΔV is the electrochemical window [V].

In 1M H_2SO_4 electrolyte, the discharge capacitance of G-CN_x-1 at a current density of 0.1 A g^{-1} was 206 F g^{-1}, obviously higher than those of G-CN_x-2 (161 F g^{-1}) and G-C (69 F g^{-1}), although the specific surface of G-CN_x-1 (404 m^2 g^{-1}) was lower than those of G-CN_x-2 (502 m^2 g^{-1}) and G-C (529 m^2 g^{-1}). Here, the capacitance values of G-CN_x-1 and G-CN_x-2 are the sum of the pseudocapacitance and the electric double-layer contribution.

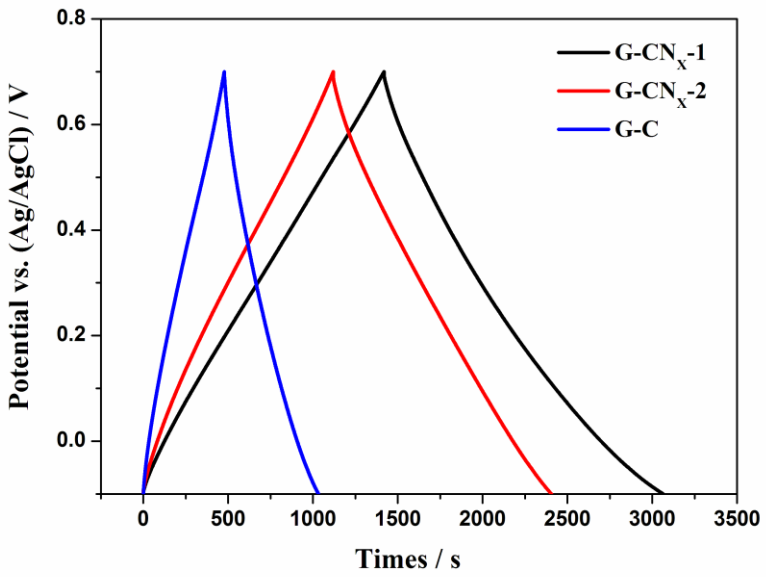

Figure 7. Galvanostatic charge/discharge curves of G-CN_x-1, G-CN_x-2 and G-C at the current density of 0.1 A g^{-1} in an electrolyte of 1M H_2SO_4 aqueous solution.

The improved capacitive performance of G-CN_x-1 than those of G-CN_x-2 and G-C is mainly due to the Faradaic redox reaction, although the different porous properties may affect the specific capacity [38], because for carbons with specific area less than 500 m^2 g^{-1}, the specific capacitance is assumed to be less than 100 F g^{-1} in 1M H_2SO_4 electrolyte at a current density of 0.1 A g^{-1} [39]. The

enhanced surface wettability by electrolyte, which is owing to basic characterization of nitrogen functionalities, also ensures a complete utilization of the exposed surfaces for charge storage [23].

Fig. 8 gave the specific capacitance obtained at various discharge current densities for all samples. It was clear that the specific capacitances of all samples decreased with the growth of current densities from 0.1 to 5 A g^{-1}, however the specific capacitances of G-CN_x-1 was still the highest.

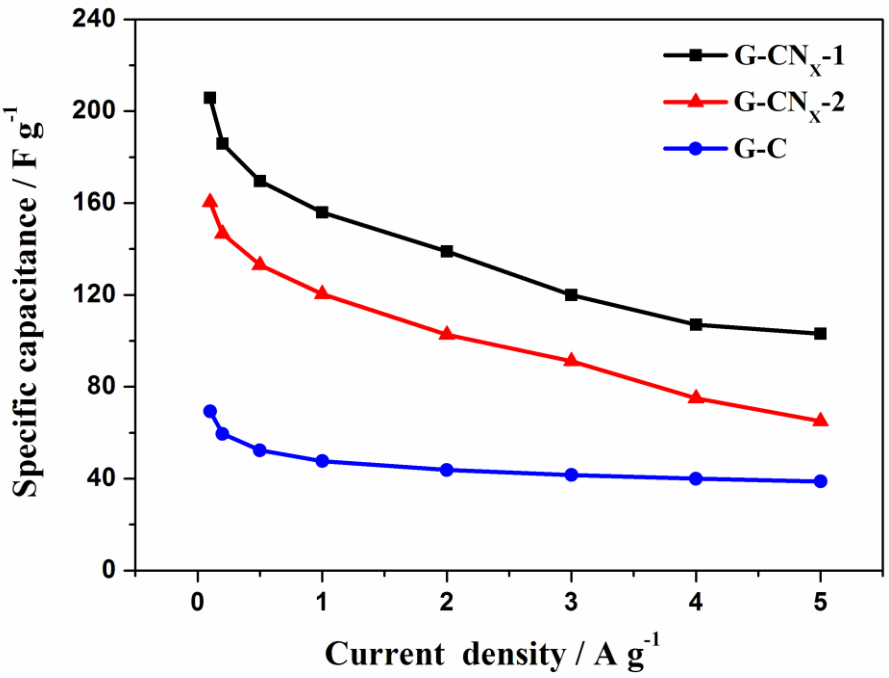

Figure 8. Specific capacitance at various discharging rates (0.1-5 A g^{-1}) of G-CN_x-1, G-CN_x-2 and G-C.

The excellent capacitive performance of G-CN_x-1 corresponds to the reasonably higher nitrogen content and the unique two-dimensional porous nanoarchitecture. The reasonably higher nitrogen content not only provides pseudocapacitance [23-29], but also enhance the surface wettability by electrolyte [23]. The unique two-dimensional porous nanoarchitecture provides shortened paths for fast electrolyte ion diffusion and large exposed surface offering more active sites for electric double-layer charge storage and redox reactions, for both are interface-bound [22,26].

4. CONCLUSIONS

Our work shows that ionic liquids can be used as nitrogen-rich carbon precursors to fabricate graphene/N-doping porous carbon composite with reasonably high amount of nitrogen (13.51 wt%) and unique two-dimensional nanoarchitecture by a simply nanocasting technology with graphene/porous silica composite as a template and pyrolyzing at moderate temperature. The

electrochemical evaluation showed that graphene/N-doping porous carbon composite with nitrogen content of 13.51 wt% exhibited greatly enhanced capacitive performances compared to the graphene/N-doping porous carbon composite with low nitrogen content (7.15 wt%) and graphene/porous carbon composite in 1M H_2SO_4 electrolyte, which clearly demonstrated the sifnificant advantage that nitrogen functionalities brought to the nanocomposite.

In addition, a loose and unique two-dimensional porous nanoarchitecture can provide fast diffusion path for electrolyte ions to migrate between the electrode and electrolyte and large exposed surface offering more active sites. Therefore, the as-prepared G-CN_x with high nitrogen content is also great promising in many other fields, such as catalysis, sensors and Li-ion battery.

ACKNOWLEDGMENT
The authors are grateful for the financial support from National Natural Science Foundation of China (No. 20973060), Shanghai Pujiang Program (No. 09PJ1403400), Fundamental Research Funds for the Central Universities, Shanghai Leading Academic Discipline Project (B502) and Shanghai Key Laboratory Project (08DZ2230500).

References

1. D. A. Dikin, S. Stankovich, E. J. Zimney, R. D. Piner, G. H. B. Dommett, G. Evmenenko, S. T. Nguyen and R. S. Ruoff, *Nature*, 448 (2007) 457
2. S. Gilje, S. Han, M. Wang, K. L. Wang and R. B. Kaner, *Nano Lett.*, 7 (2007) 3394
3. H. J. Song, N. Li, Y. J. Li, C. Y. Min and Z. Wang, *J. Mater. Sci.*, 47 (2012) 6436
4. Y. P. Zhang and C. X. Pan, *J. Mater. Sci.*, 46 (2011) 2622
5. Y. Qian, S. B. Lu and F. L. Gao, *J. Mater. Sci.*, 46 (2011) 3517
6. S. B. Yang, X. L. Feng, L. Wang, K. Tang, J. Maier and K. Müllen, *Angew. Chem. Int. Ed.*, 49 (2010) 4795
7. S. B. Yang, X. L. Feng, X. C. Wang and K. Müllen, *Angew. Chem. Int. Ed.*, 50 (2011) 5339
8. C. P. Ewels and M. J. Glerup, *Nanosci. Nanotechnol.*, 5 (2005)1345
9. Y. Shao, J. Sui, G. Yin and Y. Z. Gao, *Appl. Catal. B*, 79 (2008) 89
10. P. P. Jens, T. Arne and A. Markus, *J. Mater. Chem.*, 20 (2010) 6746
11. M. D. Nguyen, L. V. Nguyen, E. H. Jeon, J. H. Kim, M. Cheong, H. S. Kim and S. Lee, *J. Catalysis*, 258 (2008) 5
12. J. H. Davis, *Chem. Lett.*, 33 (2004) 1072
13. D. R. Macfarlane, M. Forsyth, P. C. Howlett, J. M. Pringle, J. Sun, G. Annat, W. Neil and E. I. Izgorodina, *Acc. Chem. Res.*, 40 (2007) 1165
14. J. S. Lee, N. H. Ko, H. W. Bae, D. Q. Nguyen, H. Lee, D. K. Choi, M. Cheong and H. S. Kim, *J. Membr. Sci.*, 313 (2008) 344
15. A. Tesfai, B. El-Zahab, D. K. Bwambok, G. A. Baker, S. O. Fakayode, M. Lowry and I. M. Warner, *Nano Lett.*, 8 (2008) 897
16. P. P. Jens, J. Zhang, D. S. Su, A. Thomas and M. Antonietti, *Adv. Mater.*, 22 (2010) 87
17. J. S. Lee, X. Q. Wang, H. M. Luo, G. A. Baker and S. Dai, *J. Am. Chem. Soc.*, 131 (2009) 4596
18. J. S. Lee, X. Q. Wang, H. M. Luo and S. Dai, *Adv. Mater.*, 22 (2010) 1004
19. X. Q. Wang and S. Dai, *Angew. Chem. Int. Ed.*, 49 (2010) 6664
20. L. Zhao, Y. S. Hu, H. Li, Z. X. Wang and L. Q. Chen, *Adv. Mater.*, 23 (2011) 1385
21. A. Vinu, K. Ariga, T. Mori, T. Nakanishi, S. Hishita, D. Golberg and Y. Bando, *Adv. Mater.*, 17 (2005) 1648

22. J. H. Liu and X. W. Liu, *Adv. Mater.*, (2012) DOI:10.1002/adma.201104993
23. W. R. Li, D. H. Chen, Z. Li, Y. F. Shi, Y. Wan, J. J. Huang, J. J. Yang, D. Y. Zhao and Z. Y. Jiang, *Electrochem. Commun.*, 9 (2007) 569
24. F. Beguin, K. Szostak, G. Lota and E. Frackowiak, *Adv. Mater.*, 17 (2005) 2380
25. G. Lota, B. Grzyb, H. Machnikowska, J. Machnikowski and E. Frackowiak, *Chem. Phys. Lett.*, 404 (2005) 53
26. L. Zhao, L. Z. Fan, M. Q. Zhou, H. Guan, S. Qiao, M. Antonietti and M. M. Titirici, *Adv. Mater.* 22 (2010) 5202
27. Y. H. Lee, Y. F. Lee, K. H. Chang and C. C. Hu, *Electrochem. Commun.*, 13 (2011) 50
28. K. S. Kim and S. J. Park, *Electrochim. Acta*, 56 (2011) 6547
29. D. S. Yuan, T. X. Zhou, S. L. Zhou, W. J. Zou, S. S. Mo and N. N. Xia, *Electrochem. Commun.*, 13 (2011) 242
30. W. S. Hummers and R. E. Offeman, *J. Am. Chem. Soc.*, 80 (1958) 1339
31. C. M. Yang, C. Weidenthaler, B. Spliethoff, M. Mayanna and F. Schuth, *Chem. Mater.*, 17 (2005) 355
32. M. Yoshikawa, G. Katagiri, H. Ishida and A. Ishitani, *Solid State Commun.*, 66 (1988) 1177
33. F. Tuinstra and J. L. Koening, *J. Chem. Phys.*, 53 (1970) 1126
34. A. K. M. S. Chowdhury, D. C. Cameron and M. S. J. Hashmi, *Thin Solid Films*, 332 (1998) 62
35. J. H. Kaufman, S. Metin and D. D. Saperstein, *Phys. Rev. B*, 39 (1989) 13053
36. J. Kastner, T. Pichler, H. Kuzmany, S. Curran, W. Blau, D. N. Weldon, M. Delamesiere, S. Draper and H. Zandbergen, *Chem. Phys. Lett.*, 221 (1994) 53
37. F. X. Wang, X. P. Gao, Z. W. Lu, S. H. Ye, J. Q. Qu, F. Wu, H. T. Yuan and D. Y. Song, *J. Alloys Compd.*, 370 (2004) 326
38. J. Chmiola, G. Yushin, Y. Gogotsi, C. Portet, P. Simon and P. L. Taberna, *Science*, 313 (2006) 1760
39. E. Raymundo-Piñero, K. Kierzek, J. Machnikowski and F. Béguin, *Carbon*, 44 (2006) 2498